Outlier rejection fuzzy c-means (ORFCM) algorithm for image segmentation

Fasahat Ullah SIDDIQUI,[1] **Nor Ashidi Mat ISA,**[1,*] **Abid YAHYA**[2]
[1]Imaging and Intelligent System Research Team, School of Electrical and Electronic Engineering,
University Sains Malaysia, Engineering Campus, Nibong Tebal, Penang, Malaysia
[2]School of Computer and Communication Engineering, University Malaysia Perlis,
Kuala Perlis, Perlis, Malaysia

Received: 16.11.2011 • **Accepted:** 14.05.2012 • **Published Online:** 02.10.2013 • **Printed:** 28.10.2013

Abstract: This paper presents a fuzzy clustering-based technique for image segmentation. Many attempts have been put into practice to increase the conventional fuzzy c-means (FCM) performance. In this paper, the sensitivity of the soft membership function of the FCM algorithm to the outlier is considered and the new exponent operator on the Euclidean distance is implemented in the membership function to improve the outlier rejection characteristics of the FCM. The comparative quantitative and qualitative studies are performed among the conventional k-means (KM), moving KM, and FCM algorithms; the latest state-of-the-art clustering algorithms, namely the adaptive fuzzy moving KM , adaptive fuzzy KM, and new weighted FCM algorithms; and the proposed outlier rejection FCM (ORFCM) algorithm. It is revealed from the experimental results that the ORFCM algorithm outperforms the other clustering algorithms in various evaluation functions.

Key words: Outlier rejection fuzzy c-means, fuzzy c-means, moving k-means, k-means, clustering, outlier

1. Introduction

Image segmentation is a process of subdividing an image into multiple regions of interest (ROIs) according to their sense of similarities. Clustering is an unsupervised learning method of segmentation. It categorizes a large set of patterns into disjointed clusters so that the data in each cluster are similar and extensively different from those in other clusters. This portioning process is terminated when the objects of interest in an application are completely isolated. Due to its simplicity and high speed, it is gaining more attraction in different applications, such as the identification of road signs [1], detection of the vacant vehicles in parking spaces [2], classification of the objects of interest in a digital camera image [3], characterization of the microscopic feature of bone for the determination of age at death [4], automatic dental identification system to recognize missing and unidentified persons [5], and face recognition systems, where the clustering technique is applied to extract the required region from an unwanted background region [6,7]. The background region is excluded from further processing and the execution time process can then be reduced [8,9]. In addition, the clustering is frequently used in a morphological investigation as a more reliable disease diagnostic tool, in which the size, edges, texture, and shape are measured for the segmentation of normal and abnormal tissues [10,11] or cells [12,13].

Different clustering algorithms are implemented to find a better segmentation result. One of them is known as the k-means (KM) algorithm [14]. The KM algorithm is an unsupervised and iterative method. It

*Correspondence: ashidi@eng.usm.my

assigns each point to the nearest cluster center. The center is an average of all of the points in the cluster. It is a fundamental method in many computer vision applications, whereby region extracting and recognition are 2 examples. However, it has many weaknesses, such as: 1) it is sensitive to initialization and different initial parameters could significantly produce different results (in worse cases, even poor results), and 2) objects that are far away from the cluster centers pull the centers away from the local optimum location. The fuzzy c-means (FCM) algorithm that contains soft membership was introduced in [15], which provides an opportunity for the data to belong partly to all of the clusters, if possible. Due to a degree of portioning, it becomes more flexible to locate the best possible center. The introduction of the fuzziness concept makes FCM less sensitive to initialization and it avoids the dead center problem of KM, but usually it could not minimize the intracluster variance and could not maximize the intercluster variance due to the overlapping of regions or sensitivity to the outlier.

Mashor proposed an algorithm in 2000 called the moving KM (MKM) [16]. In his work, he found 2 factors, i.e. dead center and center trapping at the local minima, as the main causes that underlie poor segmentation. The MKM minimizes these problems by keeping all of the centers in an active region and bringing the criteria of fitness into the picture, where all of the centers should have quite similar fitness. During the process, the fitness of each center is constantly checked and upon an unsatisfying condition, the cluster center with a lower variance is moved towards the region where the active center is located. Although it becomes less sensitive to initialization, it segments the data with a high intracluster variance. Further extensions have been done by transferring the elements or pixels in the appropriate clusters rather than to the cluster with a lower fitness value [17]. The approach called the adaptive fuzzy moving KM (AFMKM) incorporates a fuzzy concept to homogeneously segment an image. However, it fails to prevent the center from being trapped in local minima, which introduces poor segmentation [18].

Attempts have been made to increase the robustness of the conventional clustering algorithms. One of the previous attempts performed on the FCM shows that the Euclidean distance is very sensitive to the outlier and the problem may be reduced by replacing it with the L1 norm distance [19,20]. It is an effective approach with a limitation; the dimension must be more than one. Usually, one dimension of space (gray level) is used for image segmentation to make it cost-effective. In another study, the weight feature was introduced to adjust the sensitivity of the fuzzy membership to the outlier, such that the final solution could converge to the global optimum location [21]. This approach, called the weighted FCM (WFCM) algorithm, is performed better if the feature weight is appropriately selected [22]. Therefore, the bootstrap method based on the statistical variations in the data, called the bootstrap WFCM algorithm, is employed as the feature weight. This approach performed better than the WFCM [22]. However, both the WFCM and the bootstrap WFCM are also limited to the segmentation of an image with more than one feature vector. A few years ago, Li et al. [23] applied the concept of a weighted mean to the FCM to create a new FCM-like clustering algorithm, named the fuzzy weighted c-means (FWCM) algorithm. However, its accuracy is highly dependent on the value of the degree of fuzziness. This approach was further studied by Hung et al., who proposed a modified version of the FWCM called the new WFCM (NW-FCM) algorithm for solving similar high-dimensional multiclass pattern recognition problems [24]. On the other hand, the adaptive fuzzy KM (AFKM) algorithm was introduced to strengthen the performance of both the FCM and the KM algorithms [25]. In the AFKM, the belongingness criteria have been proposed to ensure a strong relationship between the cluster and the members within a cluster. However, the sum of the belongingness degree for a pixel among all of the clusters is not equal to 1, which could lead to the dead center problem during the segmentation process. In this study, an adaptive version of the FCM algorithm

is introduced, named the outlier rejection FCM (ORFCM). The proposed ORFCM algorithm is specifically designed to overcome the outlier problem and define nonoverlapping regions with a lower cluster variance and higher intercluster variance. The performance of the proposed algorithm is examined on 104 standard images.

The remainder of this paper is organized as follows. Section 2 outlines the background concept of the FCM and its limitations. The implementation of the proposed ORFCM algorithm is presented in Section 3. Section 4 presents the capability of the proposed algorithm on the bases of the qualitative and quantitative analyses and comparisons with other algorithms. Finally, the conclusion is presented in Section 5.

2. Background

2.1. FCM segmentation

As mentioned earlier, FCM groups the pixels of an image in overlapping regions. In terms of definition, an image $X = \{x_i\}$, $i \in \{1, 2 \ldots n\}$ is partially divided into $k$number of clusters, where x_i are the pixels of an image X and n is the total number of pixels. FCM clustering allows each pixel to belong to all of the clusters. It is based on the minimization of the following objective function:

$$FCM = \sum_{i=1}^{n} \sum_{j=1}^{k} u_{ij}^{m} \left\| x_i - c_j \right\|^2, \tag{1}$$

where u_{ij} is the degree of membership of x_i in the jth cluster and m is the degree of fuzziness, which is typically equal to 2. When m is close to 1, then the FCM algorithm is similar to the KM. A fuzzy partition is carried out through an iterative optimization of Eq. (1), by updating the cluster center c_j:

$$c_j = \frac{\sum_{i=1}^{n} \left(u_{ij}^{m} \times x_i \right)}{\sum_{i=1}^{n} u_{ij}^{m}} \tag{2}$$

and membership u_{ij}:

$$u_{ij} = \frac{1}{\sum_{p=1}^{k} \left[\frac{\|x_i - c_j\|}{\|x_i - c_p\|} \right]^{(2/m-1)}}. \tag{3}$$

The iteration will stop when $\left\| u_{ij}^{(t+1)} - u_{ij}^{t} \right\| < \varepsilon$ is fulfilled. Here, ε is the termination criterion between 0 and 1, typically set to 0.001, and t is the iteration step. Generally, the implementation of the FCM is as follows:

1. Initialize the parameters ε (i.e. termination criterion) and k (i.e. number of clusters).
2. Initialize the fuzzy partition membership function u_{ij} and let $t = 0$.
3. Calculate the cluster center c_j according to Eq. (2).
4. Let $t = t+1$ and compute the new membership function u_{ij} according to Eq. (3).
5. Repeat steps 3 to 4 until the condition $\left\| u_{ij}^{(t+1)} - u_{ij}^{t} \right\| < \varepsilon$ is fulfilled.

2.2. FCM limitations

In the conventional FCM, each point or data is associated with a membership value for each cluster. This property of FCM, with the restriction that the sum of the membership value of data point x_i in all of the clusters is equal to 1, tends to give a sufficient membership value for the outlier points (points located far from the center) to become a member of the cluster, and it increases the intracluster variance and further reduces the intercluster variance [26].

As stated above, the points are assigned to the cluster with the highest membership value, and it is sufficient to assume that it should be close to 1 or that it is at least greater than the sum of all of its remaining membership values to the other clusters. This problem is common when involving a range of data that is located between 2 neighboring clusters. To illustrate the above context, the manually generated data in the intensity range of 1 to 120 are portioned in 3 regions, c_1, c_2, and c_3, by the FCM algorithm, as shown in Figure 1. At the end of the implementation, the FCM groups the data into 3 regions, c_1, c_2, and c_3, with membership functions u_1, u_2, and u_3, respectively. As shown in Figure 1, each membership function is represented by dotted, dashed, or solid lines, respectively. For function u_1, in the range of 0 to 60, the membership is assigned to the outliers for cluster c_1 and these outliers could significantly produce insufficient effects by pulling away the center from their optimum level. The same behavior is also observed in the other clusters' membership functions, u_2 and u_3. This behavior increases the intracluster and decreases the intercluster variance.

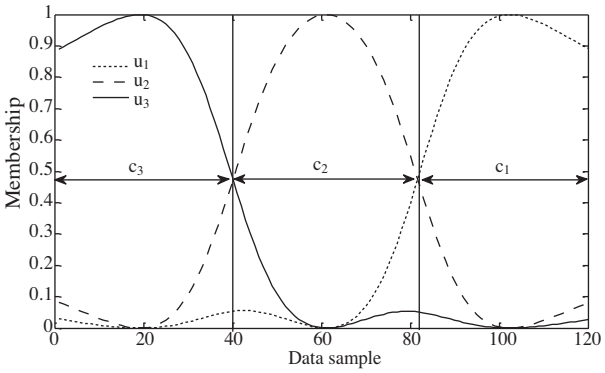

Figure 1. Membership function generated by the FCM algorithm for data of intensity range 1 to 120.

3. Proposed method

Let $X = \{x_i\}$, where $i \in \{1, 2 \ldots n\}$ denotes an image with n pixels to be partitioned into k clusters, where $2 \leq k \leq n$, and let c_j (for j = 1,2,.... k) be the jth cluster. Consider the matrix $U = (u_{ij})_{k \times n}$, called a fuzzy partition matrix, in which each element u_{ij} indicates the membership degree of each pixel in the jth cluster, c_j. The ORFCM is designed based on the minimization of the following objective function:

$$ORFCM = \sum_{i=1}^{n} \sum_{j=1}^{k} u_{ij}^{m} \beta^{\|x_i - c_j\|^2}. \tag{4}$$

The mathematical model of the ORFCM is given by:

$$\min ORFCM = \sum_{i=1}^{n} \sum_{j=1}^{k} u_{ij}^{m} \beta^{\|x_i - c_j\|^2}, \tag{5}$$

$$\begin{gathered} subject\ to: \\ u_{ij} \in [0,1] \text{ for } i = 1,2,..n \quad j = 1,2,..k \\ \sum_{j=1}^{k} u_{ij} = 1, \quad i = 1,2,...n \end{gathered} .$$

As discussed in Section 1, the Euclidean distance is very sensitive to the outliers, leading to the unrealistic nature of the FCM. In this study, the membership function of the conventional FCM algorithm is modified. The proposed ORFCM algorithm overcomes the outlier's sensitivity by changing the original Euclidean distance term in Eq. (3) (i.e. $\|x_i - c_j\|$) to $(\beta)^{\|x_i - c_j\|}$. Thus, the modified equation in calculating the membership u_{ij} is given by:

$$u_{ij} = \frac{1}{\sum_{p=1}^{k} \left[\frac{\beta^{\|x_i - c_j\|}}{\beta^{\|x_i - c_p\|}} \right]^{(2/m-1)}}. \tag{6}$$

The exponent variable β limits the partial distribution of the points among the 2 neighboring clusters rather than to all of the clusters. The β is defined as:

$$\beta = \frac{(Range\ of\ intensity\ in\ an\ image) + 1}{Maximum\ range\ of\ intensity + 1} + 1. \tag{7}$$

For an 8-bit grayscale image, Eq. (7) could be defined as:

$$\beta = \frac{(Imax - Imin) + 1}{256} + 1, \tag{8}$$

where Imax is the maximum intensity in an image and Imin is the minimum intensity in an image. The approximate range of β is between 1 and 2. If an image contains data with a large range of intensity, then the value of β is close to 2 and it could reduce the partial distribution of the points between 2 adjacent clusters. Meanwhile, if an image contains data with a small range of intensity, then the value is close to 1 and it shows more flexibility to partially distribute the points among the adjacent clusters only. Thus, it may also avoid the dead center in the small range of intensity images.

To illustrate the capability of the proposed ORFCM algorithm, the aforementioned data used to show the limitation of the FCM in Section 2.2 are revisited. Using the proposed technique, the final obtained regions, c_1, c_2, and c_3, with their membership functions, u_1, u_2, and u_3, are, respectively, shown in Figure 2a. From the graph, it can be clearly seen that the outliers have approximately a zero membership value. In addition, all of the data are partially distributed between only the 2 clusters. Here, observably, the data of the large intensity range are confined to less partial distribution between the 2 adjacent clusters. In Figure 2b, the data of the small intensity range, typically 1 to 60, are distributed in 3 regions, c_1, c_2, and c_3, with their membership functions, u_1, u_2, and u_3, respectively. It is observed that most of the data between 2 adjacent clusters are partially distributed among the adjacent clusters only. Thus, the contribution of the outliers in the central calculation has been successfully reduced, which also possibly lowers the chance of the dead center in the data of the small intensity range. Generally, the implementation of the proposed ORFCM is as follows:

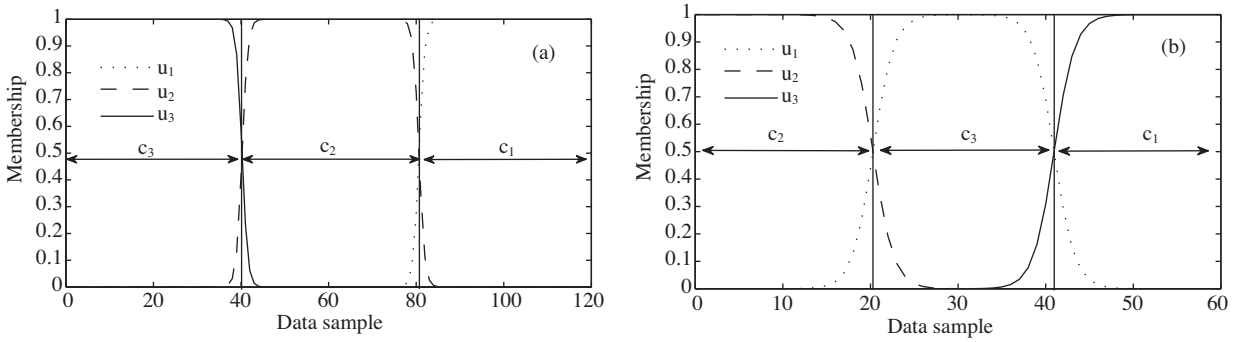

Figure 2. Membership function generated by the ORFCM algorithm for data of intensity ranges a) 1 to 120 and b) 1 to 60.

1. Initialize the parameters ε (i.e. termination criterion) and k (i.e. number of clusters).
2. Initialize the fuzzy partition membership function u_{ij} and let $t = 0$.
3. Calculate the cluster center c_j according to Eq. (2).
4. Let $t = t+1$ and compute the new membership function u_{ij} according to Eq. (6).
5. Repeat steps 3 to 4 until the condition $\left\| u_{ij}^{(t+1)} - u_{ij}^{t} \right\| < \varepsilon$ is fulfilled.

4. Experimental results and discussion

This section presents experimental results that demonstrate the robustness of the proposed ORFCM algorithm over the conventional algorithms. The performance of the proposed ORFCM algorithm is evaluated using both qualitative and quantitative analyses. This work is focused on reducing the outlier's sensitivity in a manner to group the data into clusters with less variance within the clusters and high variance among the clusters. A total of 104 images have been employed to evaluate the performance of the proposed ORFCM algorithm over the conventional KM, MKM, and FCM algorithms, and the latest state-of-the-art algorithms, namely the AFMKM, AFKM, and NW-FCM algorithms. Among them, 6 images (namely Aircraft, Camera Man, Golden Gate, Light House, Football, and Microscopic images) were selected to be visualized and to serve as testimonials to the capability of the ORFCM, as shown in Figures 3a–3f, respectively.

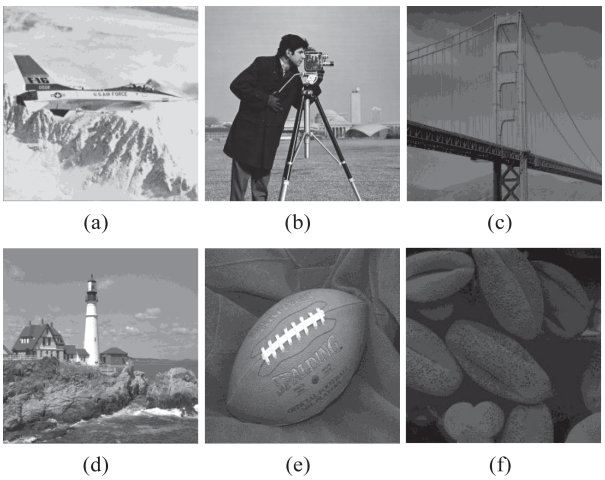

Figure 3. Original images named a) Aircraft, b) Camera Man, c) Golden Gate, d) Light House, e) Football, and f) Microscopic.

4.1. Qualitative analysis

Qualitative analysis has been proven useful to validate the ROIs from an unwanted background on the scale of human visual perception. In short, it functions to provide a visual opinion about the performance of the proposed clustering algorithm. The images in Figure 3 were implemented with the proposed ORFCM and conventional algorithms with 3, 4, and 5 clusters, as shown in Figures 4, 5, and 6, respectively. In Figures 4–6, the images in the first row are the original images, and the 2nd, 3rd, 4th, 5th, 6th, 7th, and 8th represent the resultant images after the application of the KM, MKM, FCM, AFMKM, AFKM, NW-FCM, and ORFCM algorithms, respectively. Arrows are used throughout to indicate significant differences.

4.1.1. Image segmentation in 3 clusters

Figure 4 shows the segmentation results of the tested images in 3 clusters. In Figure 4, the ORFCM images have more homogeneous background regions when a comparison is drawn with the other conventional algorithms. Specifically, the clouds in the Aircraft, Light House, and Golden Gate images, for example, are more uniformly segmented in the ORFCM when compared to the scattered segmented results of the conventional algorithms. In addition, the ORFCM reasonably segments the text written on the bottom of the Aircraft and the ropes of the Golden Gate images. The laces of the Football, as shown in Figure 4, are also successfully clustered by the ORFCM, which is not observed in the KM, MKM, FCM, AFKM, and NW-FCM. In the image named Camera Man, except for the ORFCM and AFMKM, all of the other algorithms fail to cluster the background regions smoothly. The building structure in the Camera Man image is successfully segmented by the ORFCM, NW-FCM, and FCM. In Figure 4, for all of the tested images, the MKM, AFKM, and AFMKM show the worst results in terms of the brightness and sharpness. The bad contrasts provide evidence that the MKM, AFKM, and AFMKM fail to segment images with low intracluster variance and large intercluster variance. Particularly, the AFKM has completely failed to segment any object in any of the images, except in the Microscopic and Aircraft images. Although the FCM, NW-FCM, and ORFCM show brighter and sharper resultant images, only the ORFCM successfully clusters the ROIs (objects) from unwanted backgrounds in the first 5 images. For the Microscopic image that contains a short range of intensity levels, the performance differences between the ORFCM, NW-FCM, and FCM are not easily identified. When compared to the FCM, NW-FCM, and ORFCM, the KM, MKM, AFKM, and AFMKM fail to cluster the texture in the final image labeled Microscopic.

4.1.2. Image segmentation in 4 clusters

The tested images were also segmented into 4 clusters, as shown in Figure 5. Based on Figure 5, the ORFCM has reasonably segmented the ROIs with all of the significant texture features (e.g., shapes, edges). For the results obtained by the ORFCM, text on the tail, edges of the building, and ropes of the bridge with the bridge deck rig are clearly observed in the Aircraft, Camera Man, and Golden Gate images, respectively. Furthermore, in the Aircraft, Light House, Camera Man, and Golden Gate images, the ORFCM produces a uniform background, particularly for the sky, where it is clustered in fewer regions when compared to the other algorithms. The NW-FCM and AFKM algorithms fail to segment the laces in the Football image, which are successfully segmented by the other algorithms. In addition, the AFKM produces the worst results for all of the images and segments the images into fewer clusters than the initialized number of clusters. For the Microscopic image, the KM shows the same results as produced in Section 4.1.1, which indicates the occurrence of the dead center problem. As a result, the segmented regions are not homogeneous, with many unwanted holes.

4.1.3. Image segmentation in 5 clusters

The test images having been clustered into 5 clusters are shown in Figure 6. The results obtained favor the performance of the ORFCM algorithm over the array of the KM, MKM, FCM, AFMKM, AFKM, and NW-

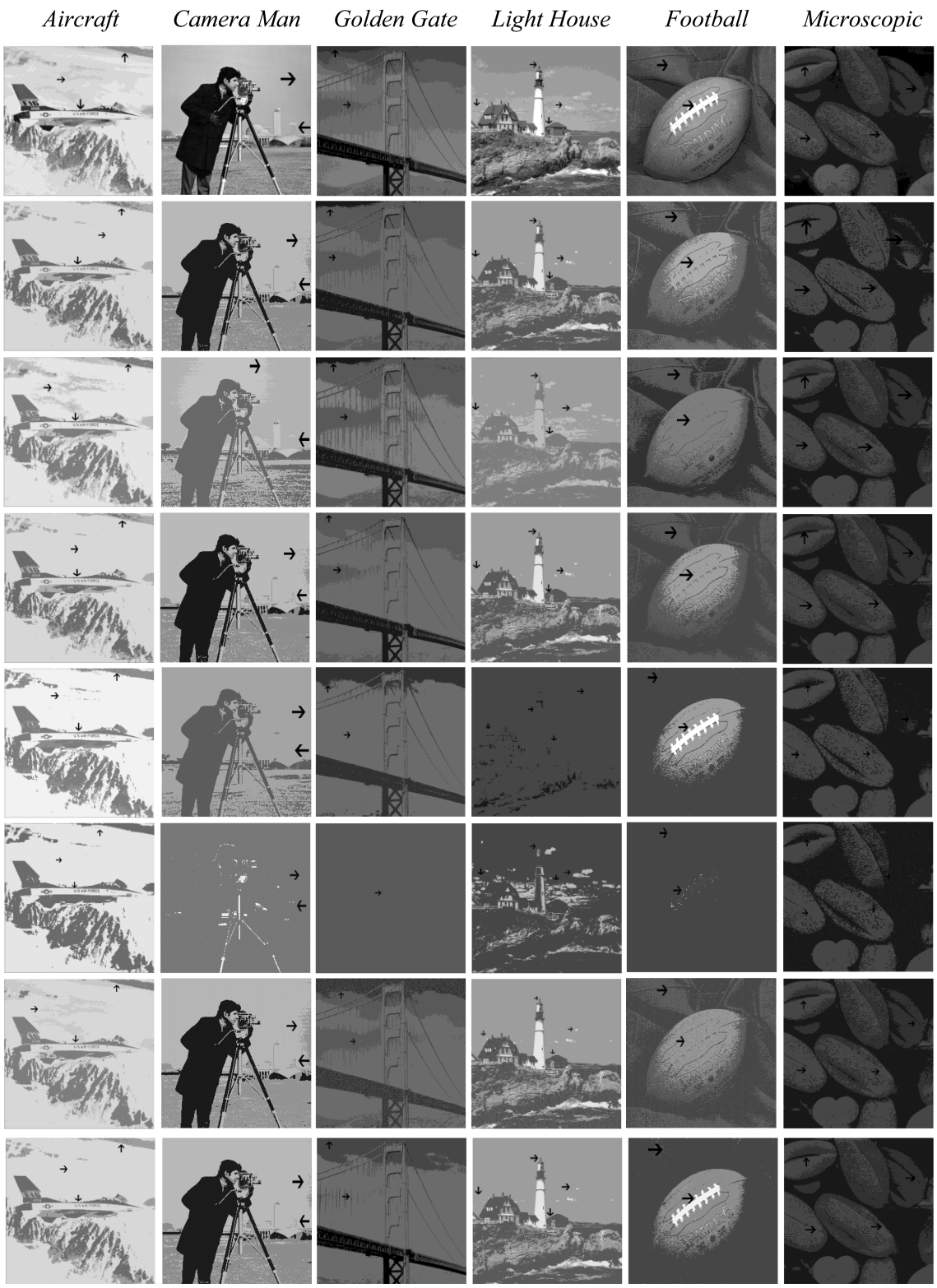

Figure 4. Segmented images in 3 clusters after applying the 1st row: original images, 2nd row: KM, 3rd row: MKM, 4th row: FCM, 5th row: AFMKM, 6th row: AFKM, 7th row: NW-FCM, and 8th row: ORFCM.

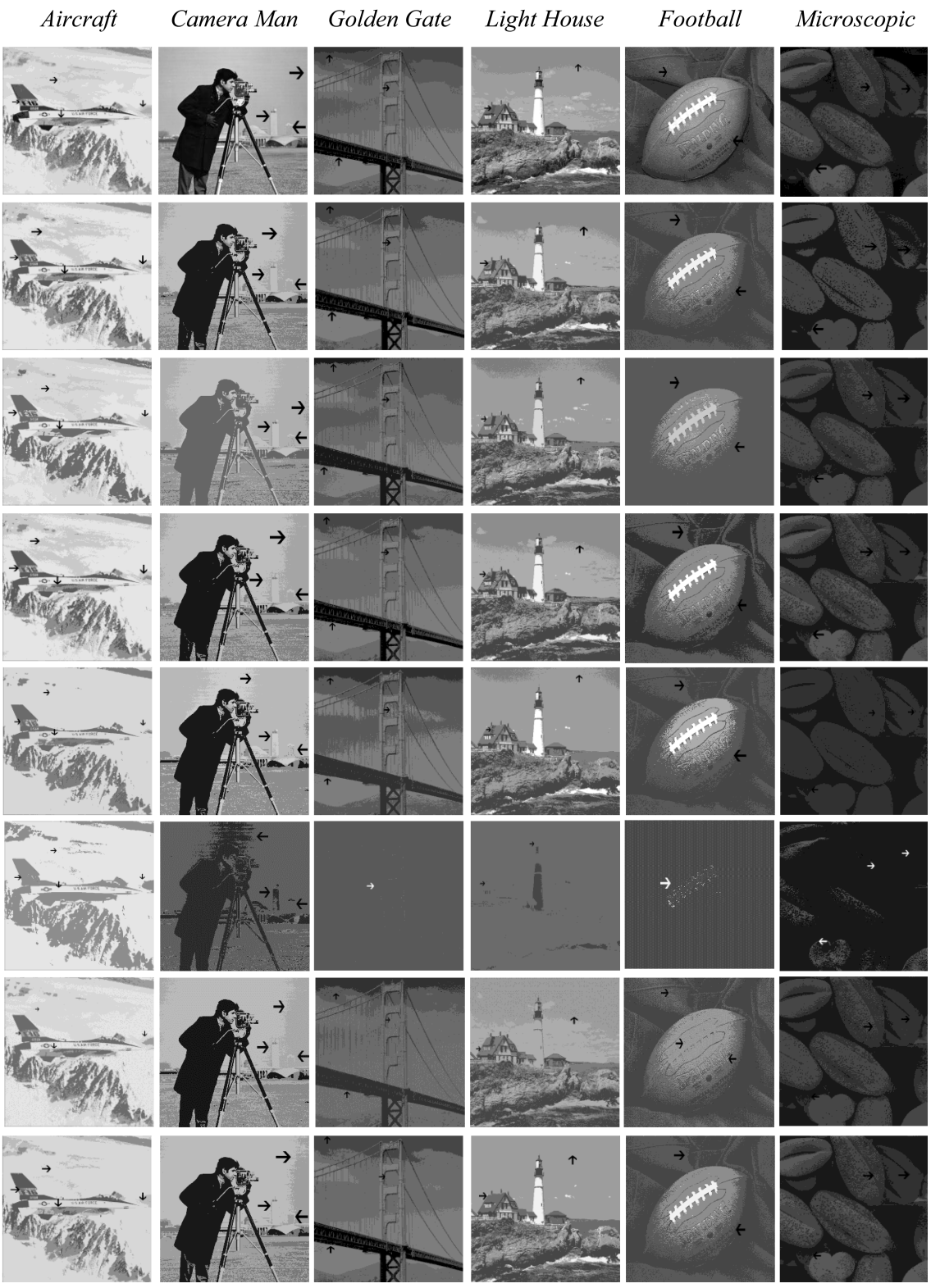

Figure 5. Segmented images in 4 clusters after applying the 1st row: original images, 2nd row: KM, 3rd row: MKM, 4th row: FCM, 5th row: AFMKM, 6th row: AFKM, 7th row: NW-FCM, and 8th row: ORFCM.

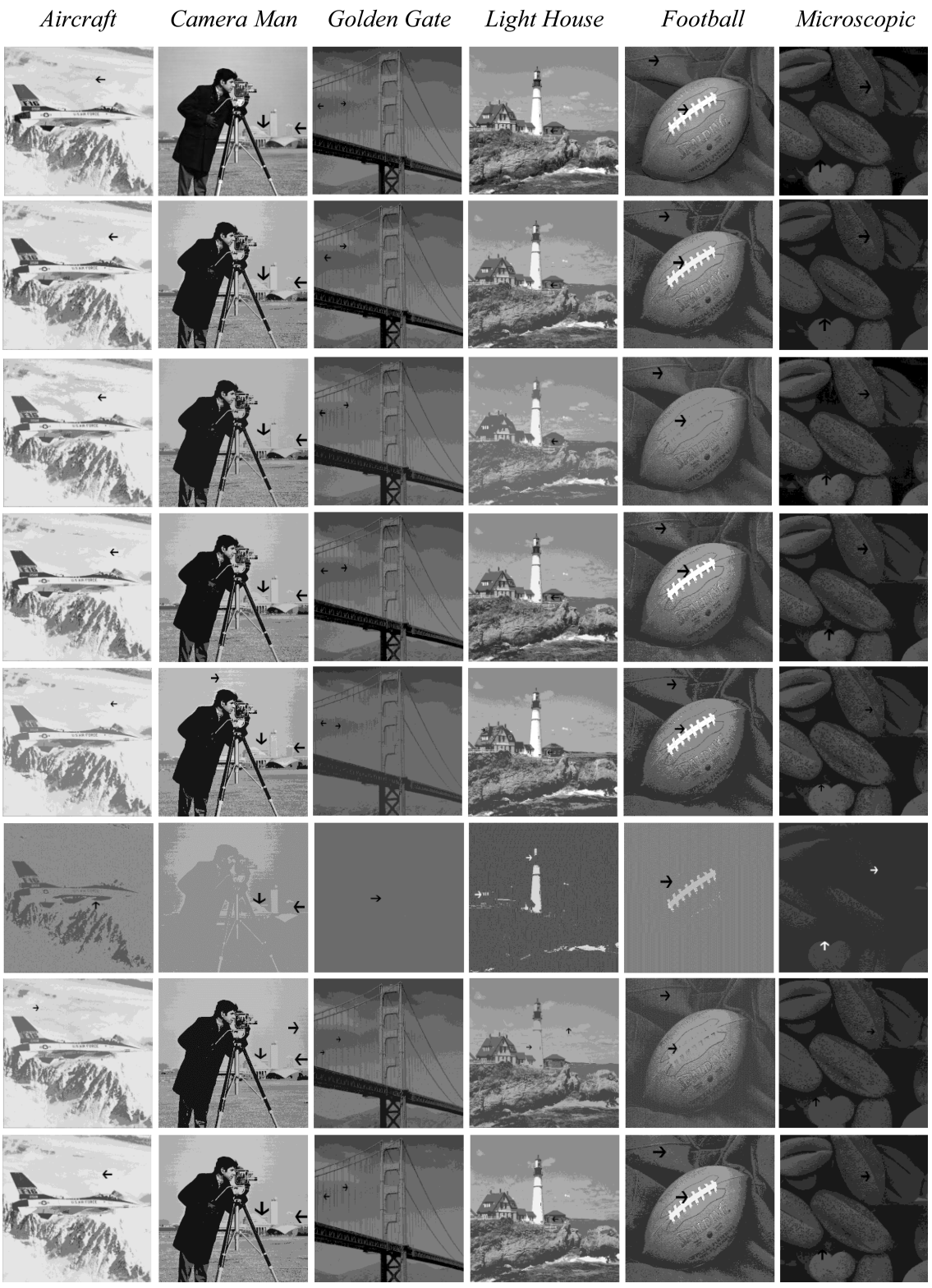

Figure 6. Segmented images in 5 clusters after applying the 1st row: original images, 2nd row: KM, 3rd row: MKM, 4th row: FCM, 5th row: AFMKM, 6th row: AFKM, 7th row: NW-FCM, and 8th row: ORFCM.

FCM algorithms. The aforementioned outcomes of Sections 4.1.1 and 4.1.2 are observed here, as well. In the Golden Gate image, the ropes are well segmented by the ORFCM when compared to the others. The uniformly clustered objects are observed by the ORFCM in the Camera Man image. For all of the images, the AFKM completely fails to segment the object of interest and produces dead centers. In the Football image, the MKM and NW-FCM produce better performance than the other algorithms, with a more homogeneous background, but the laces are still not completely observed on the football. Similarly, the scattered background region is observed in the Light House and Aircraft images by the KM. These problems have successfully been reduced by the proposed ORFCM. When compared to the KM, MKM, FCM, AFMKM, AFKM, and NW-FCM, the ORFCM in general has clustered the best possible features of the objects, with more homogeneous regions, and it has been able to avoid dead center problems.

4.2. Quantitative analysis

Quantitative analysis is a statistical analysis to numerically compute the algorithms' performances. Compared to the qualitative analysis, where the results may differ from person to person and are subjectively evaluated, a quantitative analysis measures the performance significantly without any human dependency. In this paper, 3 quantitative methods are employed to compare the performance of the proposed ORFCM algorithm with the conventional KM, MKM, FCM, and AFMKM algorithms.

To measure the accuracy of the proposed ORFCM algorithm over the conventional algorithms, the intra- and intercluster variances could be calculated using a few benchmarks. The most fundamental benchmark is the mean square error (MSE). It measures the mean of the variance within the clusters and it could be described as:

$$MSE = \frac{\sum_{j=1}^{k} \sum_{i \in c_j} \|v_i - c_j\|^2}{N}, \tag{9}$$

where the N is total number of pixels in an image and v_i is the pixels to be grouped in the jth cluster. The smaller value of the MSE reflects that the clusters contain more similar data. The findings are tabulated in Table 1 for the 5 images used in Section 4.1 and the best scores are in bold font. For the measurement of the variance among the clusters, the following formula is applied:

$$INTER = mean_{\forall q \neq r}(\|c_q - c_r\|^2), \tag{10}$$

where $q =$ *1, 2..., (k-1)* and $r = (q+1)\ldots, k$.

Here, the intercluster variance is measured by taking the mean of the differences among the clusters' centers. The large value of INTER shows that the grouped data in the clusters are significantly different from those of the other clusters. The results obtained are tabulated in Table 2 and the best scores are in bold font. The average value of the INTER and MSE for 104 test images with 3, 4, and 5 clusters are tabulated in Table 3.

In this paper, the validity Xie-Beni (VXB) function is also applied to measure the compactness and separation of the clustered data by the fuzzy-based algorithms [27]. The ratio of the compactness and separation of the data describes the VXB value, which should be smaller if the clusters are nonoverlapping and significantly different from the other clusters. It is defined as:

$$VXB = \frac{\sum_{i}^{N} \sum_{j}^{k} u_{ij}^2 \|v_i - c_j\|^2}{N \min_{\forall q \neq r} \|c_q - c_r\|^2}. \tag{11}$$

The VXB scores for the selected images are tabulated in Table 4.

Table 1. Intracluster variance (MSE) of the 6 segmented images.

Algorithm	Image	MSE for the clusters		
		3	4	5
KM	Aircraft	206.035	131.256	**84.4880**
	Camera Man	236.261	162.763	106.135
	Golden Gate	100.942	48.4598	32.0318
	Light House	305.610	207.768	112.347
	Football	330.295	116.033	76.8388
	Microscopic	82.5460	82.5460	35.3870
MKM	Aircraft	229.003	240.297	101.150
	Camera Man	1281.65	1069.83	146.829
	Golden Gate	105.953	103.858	39.5253
	Light House	721.010	229.465	328.044
	Football	499.047	342.259	404.263
	Microscopic	35.9880	21.9970	18.9450
FCM	Aircraft	207.086	133.492	84.7713
	Camera Man	237.715	163.484	106.776
	Golden Gate	98.1213	48.3278	32.7767
	Light House	307.394	209.735	113.640
	Football	339.695	116.365	77.6773
	Microscopic	35.7275	19.9714	**13.0037**
AFMKM	Aircraft	961.559	247.730	170.131
	Camera Man	1174.86	194.612	130.690
	Golden Gate	158.192	123.065	159.703
	Light House	4599.98	217.871	193.651
	Football	252.016	168.422	113.12
	Microscopic	76.7827	77.5768	17.5840
AFKM	Aircraft	687.130	724.974	6340.66
	Camera Man	4069.05	5799.31	3279.34
	Golden Gate	750.551	640.484	834.584
	Light House	4399.75	2771.23	3519.53
	Football	1857.27	1524.92	2269.29
	Microscopic	101.793	294.237	333.631
NW-FCM	Aircraft	240.639	161.453	124.274
	Camera Man	252.602	179.856	139.869
	Golden Gate	157.000	114.840	40.1922
	Light House	307.383	377.89	321.345
	Football	387.831	331.106	283.184
	Microscopic	41.0898	25.5013	20.0310
ORFCM	Aircraft	**205.607**	**129.474**	84.5635
	Camera Man	**236.116**	**160.843**	**105.993**
	Golden Gate	**92.6246**	**48.0506**	**31.9101**
	Light House	**305.593**	**189.828**	**112.032**
	Football	**230.773**	**115.514**	**76.3284**
	Microscopic	**35.3870**	**19.8858**	13.1373

Table 2. Intercluster variance (INTER) of the 6 segmented images.

Algorithm	Image	INTER for the clusters		
		3	4	5
KM	Aircraft	78.6666	77	76.8
	Camera Man	98.6666	84.1666	83.6
	Golden Gate	48	47	43.4
	Light House	103.333	89.3333	87.4
	Football	66.6666	102.5	90
	Microscopic	**35.3333**	**30.3333**	**33.2**
MKM	Aircraft	74.6666	70	74.2
	Camera Man	65.3333	52.8333	72.8
	Golden Gate	45.3333	45.1666	42.4
	Light House	45.3333	74.8333	64.4
	Football	41.3333	62.8333	36
	Microscopic	26.6666	24.3333	27.4
FCM	Aircraft	80	78.5	**78**
	Camera Man	**100.666**	85	84.4
	Golden Gate	**52**	**48.5**	**44.2**
	Light House	**104**	91.6666	89.4
	Football	60	105.5	92.6
	Microscopic	28.6666	26.8333	25.4
AFMKM	Aircraft	**91.3333**	75.3333	60
	Camera man	49.3333	**95.1666**	88.4
	Golden Gate	34.6666	34.1666	21
	Light House	23.3333	**102.5**	**94.4**
	Football	125.333	**111.5**	**112.6**
	Microscopic	20.6666	15.5	28.6
AFKM	Aircraft	82.666	55.166	24.4
	Camera Man	88.666	44.333	22
	Golden Gate	26.666	20.5	12.4
	Light House	74	47.833	85.8
	Football	**128**	81.833	51
	Microscopic	16.666	11.666	18.4
NW-FCM	Aircraft	70	68	63.8
	Camera Man	97.333	82	72.8
	Golden Gate	29.333	28.5	37
	Light House	**104**	47.333	46.6
	Football	48.666	43.166	44.2
	Microscopic	23.333	21.333	19.8
ORFCM	Aircraft	80.666	**80**	**78**
	Camera Man	98.666	83.8333	**84.8**
	Golden Gate	50.666	48.166	42.2
	Light House	**104**	95.5	87.8
	Football	118	103.166	90.8
	Microscopic	28	27	25.6

Table 3. Average of the INTER and MSE for 104 segmented images.

Algorithm	Average INTER for the clusters			Average MSE for the clusters		
	3	4	5	3	4	5
KM	84.62	82.68	**80.33**	301.4	180.4	114.9
MKM	71.30	67.69	67.28	490.1	314.0	227.6
FCM	83.05	79.88	77.51	294.9	170.2	108.8
AFMKM	**84.89**	**84.15**	75.99	941.9	452.5	257.6
AFKM	55.78	46.31	43.23	3710.3	3511.4	3512.2
NW-FCM	65.61	61.28	59.86	372.5	241.6	172.2
ORFCM	82.54	80.17	77.01	**292.3**	**167.9**	**107.8**

Table 4. VXB of the 6 segmented images.

Algorithm	Image	VXB for the clusters		
		3	4	5
FCM	Aircraft	0.22820	0.49276	0.546751
	Camera Man	0.28890	0.43875	0.47128
	Golden Gate	0.37485	0.41863	0.48109
	Light House	0.25844	0.59068	0.49493
	Football	0.51325	0.44267	0.47202
	Microscopic	0.31238	0.36032	0.39321
AFMKM	Aircraft	1.38437	2.96964	11.8139
	Camera Man	5.10747	0.57515	0.39228
	Golden Gate	1.67189	11.0739	2.07037
	Light House	9.15403	0.38327	0.60250
	Football	0.21405	0.47198	0.75681
	Microscopic	1.38044	4.07399	0.61558
AFKM	Aircraft	∞	∞	∞
	Camera Man	∞	∞	∞
	Golden Gate	3.95×10^{53}	∞	∞
	Light House	∞	∞	∞
	Football	1.74×10^{54}	∞	∞
	Microscopic	∞	∞	∞
NW-FCM	Aircraft	0.7699	1.2540	1.6340
	Camera Man	0.599	1.0419	1.3862
	Golden Gate	1.03	1.0557	1.1681
	Light House	0.258	1.1999	1.5284
	Football	0.932	1.1851	1.3131
	Microscopic	0.6243	0.7628	1.0272
ORFCM	Aircraft	**0.1984**	**0.24798**	**0.36345**
	Camera Man	**0.23917**	**0.28623**	**0.30722**
	Golden Gate	**0.27226**	**0.30162**	**0.29502**
	Light House	**0.20878**	**0.29164**	**0.33430**
	Football	**0.20680**	**0.33938**	**0.31954**
	Microscopic	**0.25287**	**0.26253**	**0.27574**

Based on the experimental results in Table 1, the ORFCM is found to be better for clustering the data with a small intracluster variance when compared to all of the other algorithms for all of the images for each number of clusters by providing the smallest MSE values. The AFKM shows the largest MSE value for almost all of the images. From Table 2, the results obtained show a comparable performance among all of the clustering algorithms. The ORFCM, AFMKM, and FCM algorithms show the best results alternately. Particularly for the Microscopic image, the KM produces quite similar INTER values for all of the clusters, which confirms that the Microscopic image is segmented into the same number of clusters for all of the cases. This phenomenon can be further seen from Figures 4–6, where the KM has segmented the Microscopic image into 3 clusters for all of the cases. This shows the occurrence of the dead center problem in the KM algorithm. The average of the MSE and INTER for the 104 test images is shown in Table 3. The lowest average values of the MSE confirm the robustness of the ORFCM to reduce the outlier effect and group the data with a small intracluster variance. Furthermore, the algorithm that has been ranked third after the AFMKM and KM, the ORFCM, is also shown to have a good capability in demonstrating a large intercluster variance.

Next, the VXB values are measured to prove the robustness of the ORFCM to cluster data in a less overlapping region. Table 4 shows that the ORFCM produces smaller VXB values for all 6 of the selected images at all of the selected values of the cluster numbers when compared to the conventional FCM, AFMKM, AFKM, and NW-FCM. After the ORFCM, the FCM, NW-FCM, and AFMKM are ranked 2nd, 3rd and 4th, respectively. In the AFKM, the infinity value of the VXB for almost all of the images indicates that the centers of 2 or more clusters have the same intensity. Due to this phenomenon, one of those clusters may get all of the members, while the others will have no members and become empty clusters or dead centers. Table 5 tabulates the statistical summary of the VXB that favors the ORFCM algorithm's performance over the other algorithms for all of the cluster numbers. In addition, graphs have been drawn between the ORFCM and its closest competitor, the FCM algorithm, to describe the ORFCM's effectiveness with 3, 4, and 5 clusters. In Figure 7, it is found that the ORFCM defines the least overlapping region for all of the images and for all of the cluster numbers, which indicates its robustness to reduce the outlier's effect.

Table 5. Statistical summary of the VXB for 104 segmented images.

Algorithm	Summary of the statistics	VXB for the clusters		
		3	4	5
FCM	Average	0.3347	0.3860	0.4196
	Maximum	0.6318	0.6282	0.6474
	Minimum	0.1421	0.1690	0.1930
AFMKM	Average	2.4219	2.9044	1.8417
	Maximum	34.582	46.849	17.620
	Minimum	0.1505	0.1495	0.1667
AFKM	Average	∞	∞	∞
	Maximum	∞	∞	∞
	Minimum	3967.9	9.57×10^{53}	6.3×10^{54}
NW-FCM	Average	0.7160	1.0145	1.4318
	Maximum	1.3683	2.9031	24.573
	Minimum	0.2539	0.3504	0.3894
ORFCM	Average	**0.2593**	**0.2796**	**0.2920**
	Maximum	**0.3619**	**0.4030**	**0.4131**
	Minimum	**0.1217**	**0.1239**	**0.1431**

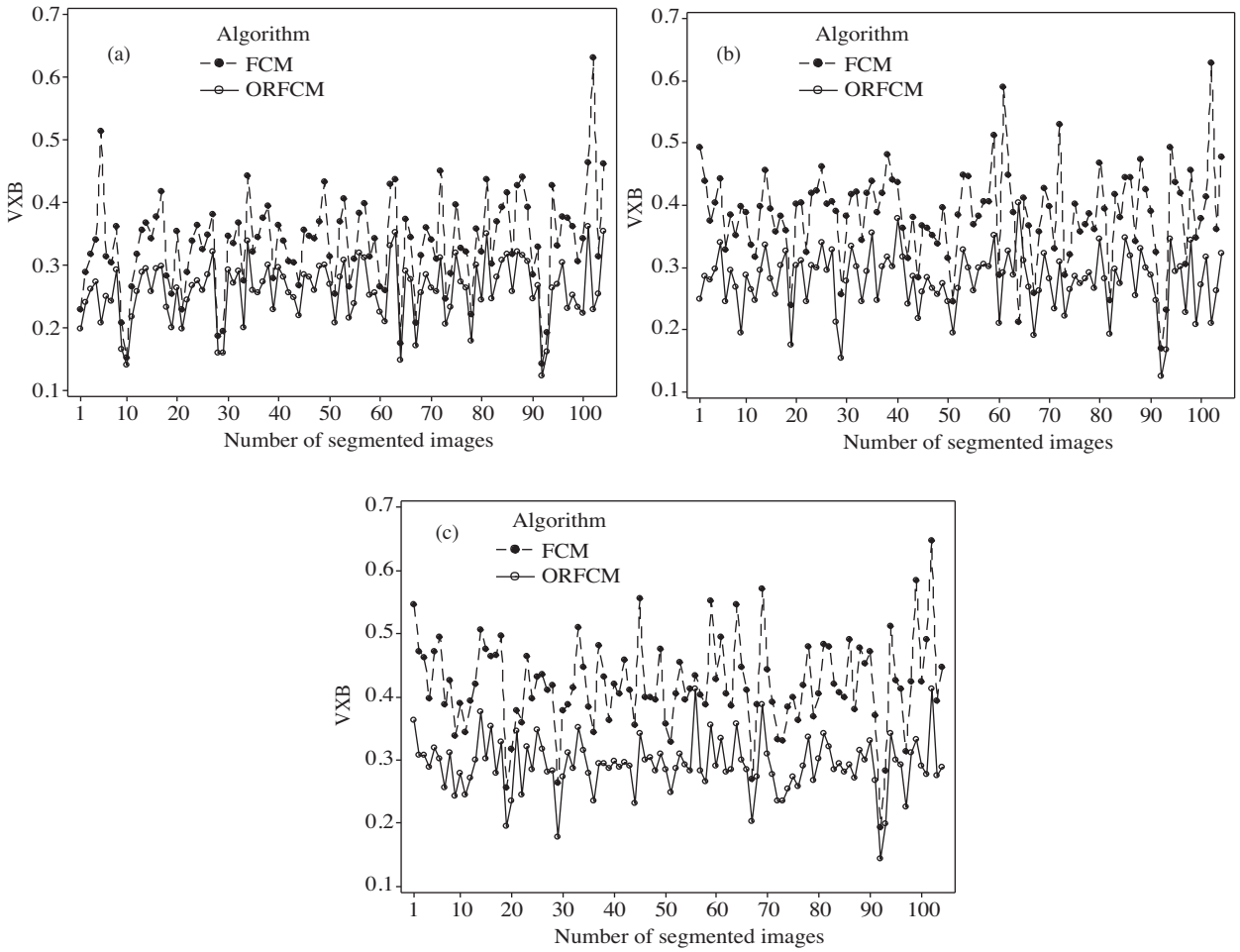

Figure 7. The VXB validity comparison between the FCM and ORFCM in clusters a) 3, b) 4, and c) 5.

In addition, the processing time of the proposed ORFCM and other conventional clustering algorithms is also measured. The processing time for the selected images is tabulated in Table 6, whereas the average processing time is tabulated in Table 7. Except for the AFKM, all of the selected fuzzy-based clustering algorithms require a long processing time to segment the image when compared to the hard membership clustering algorithms (i.e. KM and MKM). Among the fuzzy-based clustering algorithms, the proposed ORFCM algorithm is ranked second, as shown in Tables 6 and 7. In general, the proposed ORFCM algorithm has significantly segmented the images with a negligible high execution time.

Table 6. Processing time (in seconds) of the 6 segmented images.

Algorithm	Image	Processing time for the clusters		
		3	4	5
KM	Aircraft	1.6792	1.8490	3.1467
	Camera Man	0.2377	0.2058	0.5415
	Golden Gate	1.2830	1.4100	3.0059
	Light House	0.9189	0.9903	1.6955
	Football	0.4925	0.7273	0.7749
	Microscopic	**0.1430**	**0.3296**	0.8896
MKM	Aircraft	**0.2495**	13.688	10.483
	Camera Man	0.4191	0.3744	0.7691
	Golden Gate	26.678	6.3715	25.638
	Light House	8.1587	0.2949	53.210
	Football	12.504	39.144	15.440
	Microscopic	0.2572	0.6383	1.2892
FCM	Aircraft	8.2168	11.645	14.121
	Camera Man	1.7982	3.2204	3.3894
	Golden Gate	8.9701	8.9906	10.784
	Light House	10.496	14.268	12.424
	Football	6.9715	8.2329	11.603
	Microscopic	2.3315	3.2810	3.8109
AFMKM	Aircraft	0.5297	55.366	0.8027
	Camera man	0.2117	5.5066	15.063
	Golden Gate	19.438	0.5904	0.8132
	Light House	0.2634	11.491	24.379
	Football	0.4349	0.5836	7.9003
	Microscopic	2.2732	4.2566	11.201
AFKM	Aircraft	0.3223	**0.4846**	**0.6088**
	Camera Man	**0.1003**	**0.1357**	**0.1576**
	Golden Gate	**0.3001**	**0.4394**	**0.5748**
	Light House	**0.1987**	**0.4363**	**0.5639**
	Football	**0.2011**	**0.1552**	**0.1983**
	Microscopic	0.2754	0.3956	**0.5444**
NW-FCM	Aircraft	17.637	21.286	23.232
	Camera Man	3.7567	4.4886	5.2314
	Golden Gate	16.390	22.326	28.312
	Light House	8.8700	10.686	32.234
	Football	5.4192	10.394	16.643
	Microscopic	14.963	18.823	27.177
ORFCM	Aircraft	11.681	21.172	19.684
	Camera Man	1.8140	2.0023	3.3127
	Golden Gate	9.2304	9.9510	14.707
	Light House	9.2245	9.4364	11.961
	Football	7.4190	10.032	12.803
	Microscopic	3.6462	3.3936	6.8116

Table 7. Average processing time (in seconds) for 104 segmented images.

Algorithm	Average processing time for the clusters		
	3	4	5
KM	0.7458	1.2901	1.9996
MKM	10.248	10.621	10.718
FCM	5.9813	7.8723	10.708
AFMKM	6.9501	11.358	29.367
AFKM	**0.2493**	**0.3528**	**0.4575**
NW-FCM	13.744	20.071	26.453
ORFCM	6.5341	8.4583	11.732

5. Conclusion

In this paper, an ORFCM algorithm has been introduced as a modified version of the conventional FCM algorithm. Unlike the conventional membership functions in the FCM, the proposed membership function is less sensitive to the outlier. The ORFCM has introduced the exponent operation of the Euclidean distance in its membership function in order to assign a lower value to any far-located point that could neutralize the outlier's effect. Both qualitative and quantitative analyses have been performed on the conventional clustering algorithms and the proposed ORFCM algorithm. When compared to the conventional algorithms, the proposed algorithm is found to be more efficient and robust against the outlier, and it can better assist in segmenting the images with a small intracluster variance and large intercluster variance. Furthermore, the experimental results show that the ORFCM algorithm achieves more consistent segmentation accuracy, irrespective of the number of clusters.

Acknowledgment

This work was supported by the Universiti Sains Malaysia short-term grant entitled "Fuzzy logic based segmentation technique for determination of breast tumour on mammogram image".

References

[1] A. Krishnan, C. Lewis, D. Day, "Vision system for identifying road signs using triangulation and bundle adjustment", IEEE Conference on Intelligent Transportation Systems, pp. 36–41, 2009.

[2] H. Ichihashi, A. Notsu, K. Honda, T. Katada, M. Fujiyoshi, "Vacant parking space detector for outdoor parking lot by using surveillance camera and FCM classifier", IEEE International Conference on Fuzzy Systems, pp. 127–134, 2009.

[3] E. Lee, W. Kang, S. Kim, J. Paik, "Color shift model-based image enhancement for digital multifocusing based on a multiple color-filter aperture camera", IEEE Transactions on Consumer Electronics, Vol. 56, pp. 317–323, 2010.

[4] Z.Q. Liu, H.L. Liew, J.G. Clement, C.D.L. Thomas, "Bone image segmentation", IEEE Transactions on Biomedical Engineering, Vol. 46, pp. 565–573, 1999.

[5] X. Li, A. Abaza, D.E. Nassar, H. Ammar, "Fast and accurate segmentation of dental X-ray records", Lecture Notes in Computer Science, Vol. 3832, pp. 688–696, 2005.

[6] M. Hu, Q. Zhang, Z. Wang, G. Wu, "An improved fuzzy c means and Kathunen-Loeve transform method for face detection", Proceedings of the 3rd International Conference on Innovative Computing Information and Control, pp. 201–204, 2008.

[7] H. Gu, G.D. Su, C. Du, "Fuzzy and ISODATA classification of face contours", Proceedings of the International Conference on Machine Learning and Cybernetics, pp. 3568–3573, 2004.

[8] L. Ianming, Y. Xue, T. Yahagi, "A method of face recognition based on fuzzy c-means clustering and associated sub-NNs", IEEE Transactions on Neural Networks, Vol. 18, pp. 150–160, 2007.

[9] R. Gottumukkal, V.K. Asari, "Real time face detection from color video stream based on PCA method", Proceedings of the 32nd Workshop on Applied Imagery Pattern Recognition, pp. 146–150, 2003.

[10] M. Ceylan, Y. Özbay, O.N. Uçan, E. Yıldırım, "A novel method for lung segmentation on chest CT images: complex-valued artificial neural network with complex wavelet transform", Turkish Journal of Electrical Engineering and Computer Sciences, Vol. 18, pp. 613–624, 2010.

[11] B. Sahiner, N. Petrick, C.H. Ping, L.M. Hadjiiski, C. Paramagul, M.A. Helvie, M.N. Gurcanc, "Computer-aided characterization of mammographic masses: accuracy of mass segmentation and its effects on characterization", IEEE Transactions on Medical Imaging, Vol. 20, pp. 1275–1284, 2001.

[12] N.A.M. Isa, M.Y. Mashor, N.H. Othman, "Comparison of segmentation performance of clustering algorithms for pap smear images", Proceedings of the International Conference on Robotics, Vision, Information and Signal processing, pp. 118–125, 2003.

[13] S. Wang, M. Wang, "A new detection algorithm (NDA) based on fuzzy cellular neural networks for white blood cell detection", IEEE Transactions on Information Technology in Biomedicine, Vol. 10, pp. 5–10, 2006.

[14] J.B. MacQueen, "Some methods for classification and analysis of multivariate observations", Proceedings of the 5th Berkeley Symposium on Mathematical Statistics and Probability, pp. 281–297, 1967.

[15] J.C. Bezdek, Pattern Recognition with Fuzzy Objective Function Algorithms, New York, Plenum Press, 1981.

[16] M.Y. Mashor, "Hybrid training algorithm for RBF network", International Journal of the Computer, the Internet and Management, Vol. 8, pp. 50–65, 2000.

[17] N.A.M. Isa, A.S. Samy, U.K. Ngah, "Adaptive fuzzy moving k-means clustering algorithm for image segmentation", IEEE Transactions on Consumer Electronics, Vol. 55, pp. 2145–2153, 2009.

[18] F.U. Siddiqui, N.A.M. Isa, "Enhanced moving k-means (EMKM) algorithm for image segmentation", IEEE Transactions on Consumer Electronics, Vol. 57, pp. 833–841, 2011.

[19] P.R. Kersten, "Fuzzy order statistics and their application to fuzzy clustering", IEEE Transactions on Fuzzy Systems, Vol. 7, pp. 708–712, 1999.

[20] R. Hathaway, J.C. Bezdek, Y. Hu, "Generalized fuzzy c-means clustering strategies using L_P norm distances", IEEE Transactions on Fuzzy Systems, Vol. 8, pp. 576–582, 2002.

[21] X. Wang, Y. Wang, L. Wang, "Improving fuzzy c-means clustering based on feature-weight learning", Pattern Recognition Letters, Vol. 25, pp. 1123–1132, 2004.

[22] W.L. Hung, M.S. Yang, D.H. Chen, "Bootstrapping approach to feature-weight selection in fuzzy c-means algorithms with an application in color image segmentation", Pattern Recognition Letters, Vol. 29, pp. 1317–1325, 2008.

[23] C.H. Li, W.C. Huang, B.C. Kuo, C.C. Hung, "A novel fuzzy weighted c-means method for image classification", International Journal of Fuzzy Systems, Vol. 10, pp. 168–173, 2008.

[24] C.C. Hung, S. Kulkarni, B.C. Kuo, "A new weighted fuzzy c-means clustering algorithm for remotely sensed image classification", IEEE Journal of Selected Topics in Signal Processing, Vol. 5, pp. 543–553, 2011.

[25] S.N. Sulaiman, N.A.M. Isa, "Adaptive fuzzy-k-means clustering algorithm for image segmentation", IEEE Transactions on Consumer Electronics, Vol. 56, pp. 2661–2668, 2010.

[26] B. Thomas, G. Raju, W. Sonam, "A modified fuzzy c-means algorithm for natural data exploration", Proceedings of World Academy of Science: Engineering & Technology, Vol. 49, pp. 478–481, 2009.

[27] X.L. Xie, G. Beni, "A validity measure for fuzzy clustering", IEEE Transactions on Pattern Analysis and Machine Intelligence, Vol. 13, pp. 841–847, 1991.